new peaks appearing at 2936 and 1716 cm^{-1} contributed hydrocarbon and carbonyl groups of the monomer. It is clear that graft-polymerization of MOI-oxime is well conducted.

After HAp nanoscaled particles were suspended in toluene/isopropanol (9/1), a poly(MOI-oxime)-grafted SF was soaked in the suspended solution for 1 h at room temperature to be adsorbed on the SF. The SF adsorbed with the particles was washed by stirring in ethanol. This fabric with HAp was heated at 140°C for 20 min in vacuum at 1 mmHg for the deblocking of MOI-oxime and the reaction between the HAp particles and the isocyanate group of the grafted polymer. The composite was washed by using an ultrasonic generator for 3 min (output: 20 kHz, 35 W) to remove excess adsorbed HAp particles attached to ones in the same solution. Finally, the composite was washed in a great amount of distilled water for one day to remove the residual organic solvents used in the synthetic process.

The surface morphologies of HAp nanoparticles coated on a SF fiber explained in the next paragraph. To prove indirectly the formation of the urethane linkage between HAp particles and MOI-oxime, the reaction of the particles with the MOI-oxime monomer was carried out. Briefly, the HAp nanoparticles adsorbed with MOI-oxime were heated at 140°C for 20 min in vacuum at 1 mmHg and the product was washed by acetone to remove the unreacted reagents. Figure 9 shows the diffuse reflectance FT-IR spectra of the original and (MOI-oxime)-modified HAp nanoparticles. The spectrum of the (MOI-oxime)-modified HAp (Fig. 9(b)) shows additional absorption bands, with respect to the original particle spectrum, due to C-H stretch at 2978, C=O stretch of the ester group at 1724, C=O stretch of the urethane group at 1653, and N–H bending at 1575 cm^{-1}. This result is in accord with Liu's paper [58]. By heating in vacuum, the formation of the urethane linkage follows the release of oxime from MOI-oxime to generate the isocyanate groups [56], because the deblocking temperature of MOI-oxime is 140°C and the boiling point of oxime is 60°C. From the spectrum, it is estimated indirectly that HAp particles might be coupled with the isocyanate groups in poly (MOI-oxime)-grafted SF by the urethane linkage. It is possible to lower the reaction temperature by using MOI blocked with phenol or imidazole, for the deblocking temperature of these agents is 110–130°C [56]. This reaction system is, therefore, a unique method of fixing HAp on the polymer substrate.

3.2.2. Alkoxysilyl Group

Graft-polymerization with MPTS monomer having an alkoxysilyl group on SF fibers with 100 μm of length was conducted by free radical initiation. Initially, 1.8 mmol of the MPTS and 0.18 mol of a nonionic surfactant, pentaethylene glycol dodecyl ether, were thoroughly mixed and added to 50-ml thick-walled polymerization tubes. Subsequently, 0.18 mmol of APS in 6.0 ml of distilled water and 600 mg of SF fibers was added to the tubes. The tube was degassed by freezing, evacuated three times, and then sealed. Graft-polymerization was conducted at 50°C for different periods. Poly(MPTS)-grafted SF were collected from the reaction system, washed with 300 ml of dry-methanol and filtrated by a filter with a 5- μm cut-off point to remove unreacted monomers and homopolymers and dried by vacuum for 1 h at 60°C. After the HAp particles were suspended in a toluene/methanol (9/1) mixture solvent, a poly(MPTS)-grafted SF was soaked in the suspended solution for 1 h at room temperature to be adsorbed on the SF. The SF adsorbed with the HAp particles was washed by stirring in methanol and filtered by a filter with a 5- μm cut-off point to remove unreacted HAp particles. The fibers adsorbed with HAp were heated at 120°C for 2 h in vacuum at 1 mmHg for a reaction between the HAp surface and the alkoxysilyl groups of the graft polymers. The composite was washed by using an ultrasonic generator for 3 min (output: 20 kHz and 35 W) to remove excess adsorbed HAp particles attached to ones in ethanol. Finally, the composite was washed in a great amount of distilled water for one day to remove the residual organic solvents used in the synthetic process.

Graft-polymerization with MPTS possessing alkoxysilyl groups coupled with hydroxyl groups on the HAp surface on the SF substrate through a one-step procedure was conducted. Figure 10 shows the ATR FT-IR spectra of the poly(MPTS) homopolymer, unreacted SF and

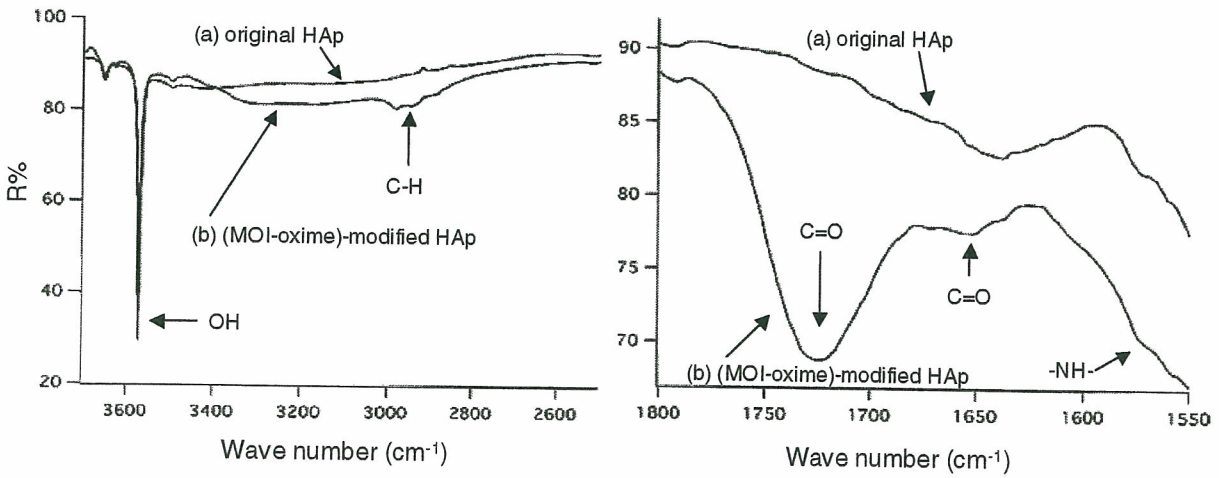

Figure 9. Diffuse reflectance FT-IR spectra of (a) original and (b) (MOI-oxime)-modified calcined HAp nanoparticles.

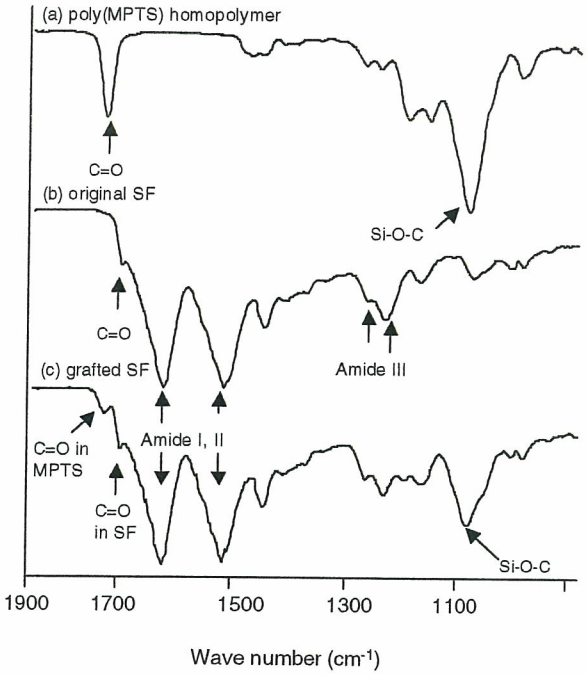

Figure 10. ATR FT-IR spectra of (a) poly(MPTS) homopolymer, (b) SF fiber, and (c) poly(MPTS)-grafted SF. Reprinted with permission from [21], T. Furuzono et al., *J. Artif. Organs* 7, 137 (2004). © 2004, Springer.

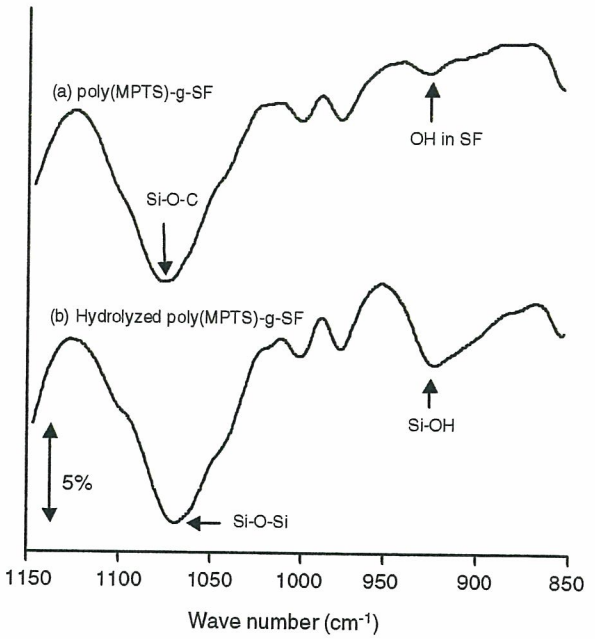

Figure 11. ATR FT-IR spectra of (a) poly(MPTS)-grafted SF just after preparation and (b) hydrolyzed poly(MPTS)-grafted SF. Reprinted with permission from [21], T. Furuzono et al., *J. Artif. Organs* 7, 137 (2004). © 2004, Springer.

the poly(MPTS)-grafted SF having 14.3 wt% of weight gain against intact SF. Typical peaks in the poly(MPTS) homopolymer can be seen at 1725 and 1076 cm^{-1} ascribed the C=O stretching vibration of ester groups and the Si-O-C stretching vibration of alkoxysilyl groups, respectively (Fig. 10(a)). The peaks at 1621, 1514, and 1260/1230 cm^{-1} were attributed to amide I, II, and III, respectively, which are the typical absorbances of the SF substrate, as shown in Figure 10(b). After graft-polymerization with poly(MPTS), a peak contributing to Si-O-C of the graft-polymer remains at 1076 cm^{-1} in Figure 10(c). Figure 11 shows ATR FT-IR spectra of the poly(MPTS)-grafted SF just after preparation and the sample treated by hydrolysis with water in an autoclave. In the spectrum of the poly(MPTS)-grafted sample (a), the Si-O-C stretching vibration attributed to the graft-polymer at 1076 cm^{-1} and the OH stretching vibration belonging to the SF substrate at 926 cm^{-1} were recognized. However, two new peaks appear at 1068/922 cm^{-1} belonging to the Si-O-Si and Si-OH stretching vibrations, respectively, in the spectrum of the hydrolyzed sample (b). This means that the alkoxysilyl groups of the graft-polymers just after preparation avoided hydrolysis, and maintained their activity in coupling with the hydroxyl groups on the HAp surface regardless of using water as the reaction solvent. The surfactant in the reaction solvent was effective in protecting the active groups from hydrolysis. In our previous study, graft-polymerization having alkoxysilyl groups was achieved through a vinyl bond of 2-methacryloxyethyl isocyanate (MOI) bonded on the SF substrate in anhydrous organic solvents via a two-step procedure [19]. It can be mentioned that the alternative graft-polymerization system in this section is technically easier and more advantageous compared to the former method due to using water as the solvent and the single-reaction procedure.

Figure 12 shows the ATR FT-IR spectrum of the calcined HAp nanoparticles coated on poly(MPTS)-grafted SF. The weight gain of HAp particles coated on SF was 13.2 wt% determined by a thermogravimetric analysis (TGA). The peak at 3572 cm^{-1} belongs to the OH stretching vibration of highly crystalline HAp coated on SF. This peak is very small because a signal intensity of the ATR FT-IR spectrum shows the specific character that is weaker in a higher wave-number region than that in a lower region. The peaks at 1091 and 1052 cm^{-1} reflect $\nu_3(PO_4^{3-})$ of the HAp crystals. The peak at 3281 cm^{-1} shows OH stretching of amino acids in SF because there are many hydroxyl residues such as 10.63 mol% of Ser, 4.97 mol% of Tyr, and 0.89 mol% of Thr in SF. Although the bands attributed to the Si-O-Si stretching vibration at 1068 cm^{-1} or Si-OH at 922 cm^{-1} generated by hydrolysis of poly(MPTS) cannot be seen due to an overlap of the peaks attributed to the PO_4^{3-} stretching vibration of HAp at around 1100–900 cm^{-1}, the peaks of amide I/II and two C=O from poly(MPTS) and the SF substrate at 1621/1514 and 1725/1696 cm^{-1}, respectively, can be clearly observed. This means the coating of HAp particles did not fully and thickly cover the surface of grafted SF. The existence of covalent bonds between the HAp particles and the poly(MPTS)-grafted SF was estimated by an indirect method using an FT-IR measurement [18].

As the evidence of existence of covalent linkage, in the FT-IR spectrum of the heating product of the mixture with the HAp nanoparticles and the MPTS monomer at 120°C

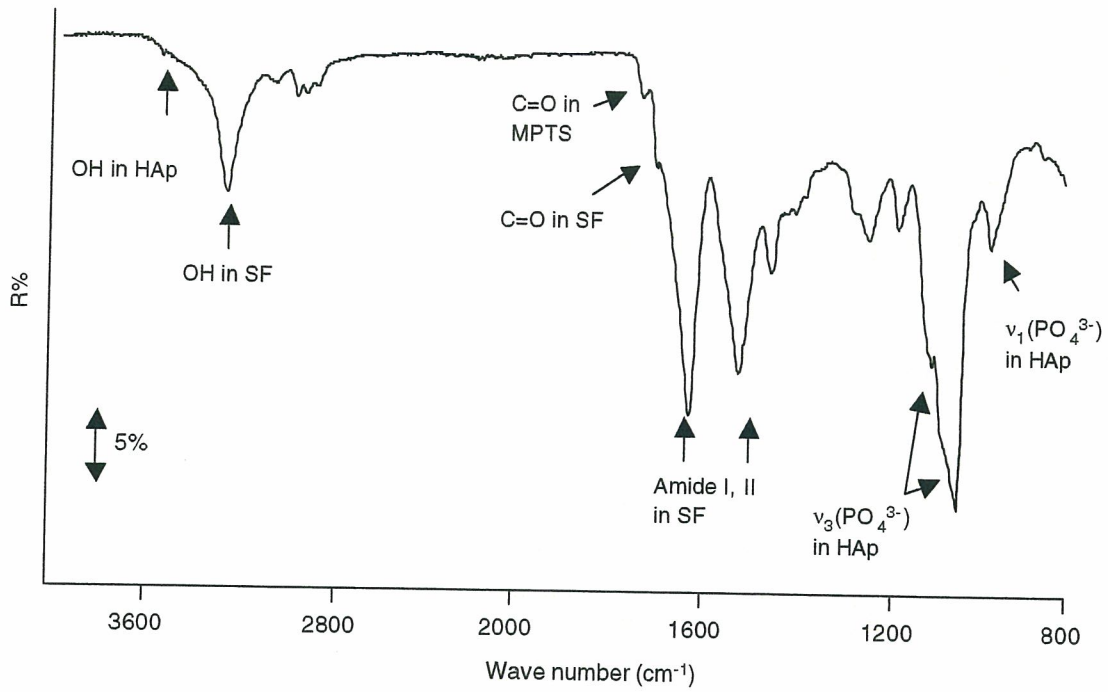

Figure 12. ATR FT-IR spectrum of calcined HAp particles covalently coated on SF fibers. Reprinted with permission from [21], T. Furuzono et al., *J. Artif. Organs* 7, 137 (2004). © 2004, Springer.

for 2 h in vacuum, a new peak appeared at 1043 cm^{-1} [18]. This band is known as the sign belonging to an Si-O stretching vibration from the covalent bond between the HAp and silane coupling agent [52].

Figure 13 shows an SEM photograph of the HAp-coated SF fiber with 13.1 ± 1.2 wt% ($n = 4$) in the composite determined by TGA. The weight gain of HAp particles on the SF fiber increased about 5 times compared to that on the SF fabric, 2.8 ± 0.5 wt% by the same preparation conditions. This means that it is hard for nano-HAp particles to penetrate into and coat on gaps between fibers in the SF fabric.

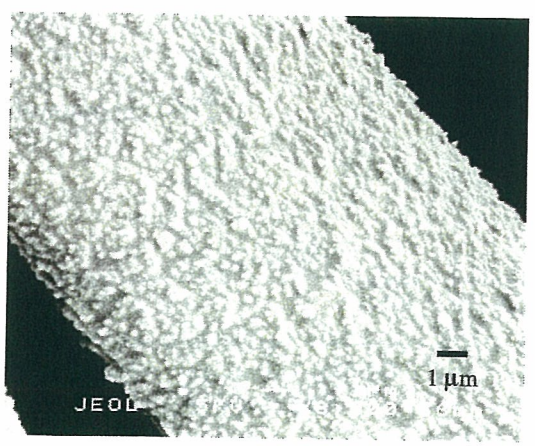

Figure 13. SEM photograph of calcined HAp nanoparticles covalently coated on an SF fiber. Reprinted with permission from [21], T. Furuzono et al., *J. Artif. Organs* 7, 137 (2004). © 2004, Springer.

In other words, a fiber cut approximately 100 μm in length was more effective for the coating than that of a fabric form. The HAp particles separated or aggregated into several crystals under SEM observation. Aggregation was easy because the HAp monoparticle has an *a*-plane with a cationic charge and a *c*-plane with an anionic charge in a monocrystal [59]. It was difficult, therefore, to prepare perfect monolayer with HAp nanoparticles separately on the SF surface.

3.3. HAp Coating by Ionic Bonding

3.3.1. Carboxyl Group

In the former subsections, the coupling method between HAp nanoparticles and a polymer substrate through covalent linkage was mentioned. This synthetic way needs, however, one more step, which is thermal treatment above 100°C in a vacuum to connect HAp to SF by covalent linkage, besides the physical adsorption of HAp on the SF. This system is not useful when applying it to the non-heat-resistant biomedical material such as polyethylene and is industrially disadvantageous. In this subsection, to couple HAp particles and SF under a nonheat condition, therefore, we applied graft-polymerization with 4-methacryloyloxyethyl trimellitate anhydride (4-META) onto the SF by free radical initiation. The 4-META has already been applied to resin monomers for dental surgery and is harmless to a living body. Moreover, the methyl methacrylate (MMA) resin with 4-META had larger tensile bond strength compared with the MMA resin without 4-META because of the strong affinity between HAp and 4-META [60]. Here, we report on the synthesis and bioactivity of the novel HAp/SF composite using 4-META.

Graft-polymerization with 4-META onto the SF was conducted by free radical initiation [57], with 273.80 mg (0.9 mmol) of the 4-META monomer, 41 mg (0.18 mmol) of APS, and 73 mg (0.18 mmol) of the surfactant were mixed in 6.0 ml of distilled water. The 74.94 mg of the SF fabric (18 mm in diameter) was immersed in the reaction mixture in 50-ml thick-walled polymerization tubes. The tubes were degassed by freezing and evacuating three times and then sealed. Graft-polymerization was conducted at 50°C for different periods. The poly(4-META)-grafted fabrics were collected from the reaction system, washed with acetone followed by washing with distilled water to remove unreacted monomers and homopolymers, and finally dried by vacuum for 24 h at room temperature.

The poly(4-META)-grafted SF was immersed in a 0.01 M potassium hydroxide aqueous solution for 10 min and the five-member ring of this SF was opened and ionized. After HAp nanoscaled particles were suspended in toluene/methanol (8.8/1), an ionized poly(4-META)-grafted SF was soaked in the suspended solution for 1 h at room temperature to be adsorbed on the SF. The SF adsorbed with the particles was washed by stirring in acetone to remove the solvent. The composite was washed in distilled water by using an ultrasonic generator for 3 min (output: 20 kHz, 35 W) to remove excess adsorbed HAp particles. Finally, the composite was freeze-dried by vacuum for one day to evaporate the residual water.

Figure 14 shows the ATR-FTIR spectra of the 4-META monomer, the original SF, the poly(4-META)-grafted SF, and the ionized poly(4-META)-grafted SF. The peaks at 1621, 1514, and 1260/1230 cm^{-1} were attributed to amide I, II, and III, respectively, which are the typical absorbances of the SF substrate as shown in Figure 14(b). After modification with the 4-META monomer (Fig. 14(c)), new peaks contributing to the monomer appeared due to the C=O stretching vibration of –CO–O–CO– at 1724 cm^{-1} and ester groups at 1696 cm^{-1}, and the C-O stretching vibration of ester groups at 1158 cm^{-1}. After ionization of the grafted SF (Fig. 14(d)), the peak of the C=O stretching vibration of –CO–O–CO– disappeared and new peaks at 1392 and 1367 cm^{-1} attributed to the symmetric vibration of –COO– appeared.

To estimate indirectly the formation of ionic interaction, HAp particles connected with ionized 4-META were prepared. The HAp particles were adsorbed with 4-META, ionized by a 0.1 M potassium hydroxide aqueous solution in toluene/methanol (8.8/1) for 1 h. The reactant was washed with distilled water to remove the unreacted reagents and dried by heating at 120°C under vacuum.

In Figure 15, the solid line shows the difference FT-IR spectrum which subtracts the original HAp from the HAp particles with ionized 4-META. The peak of 1368 cm^{-1} demonstrates the existence of $-COO^-$. This absorption band shifted by 6 cm^{-1} to a lower side of wave number in comparison with ionized 4-META (dotted line, 1374 cm^{-1}). This shift suggests that carboxylate groups in ionized 4-META interacted with Ca^{2+} ions on the surface of HAp [61, 62]. From these spectra, it is estimated indirectly that HAp nonoparticles might be coupled with $-COO^-$ groups in the ionized poly(4-META)-modified SF by the ionic interaction.

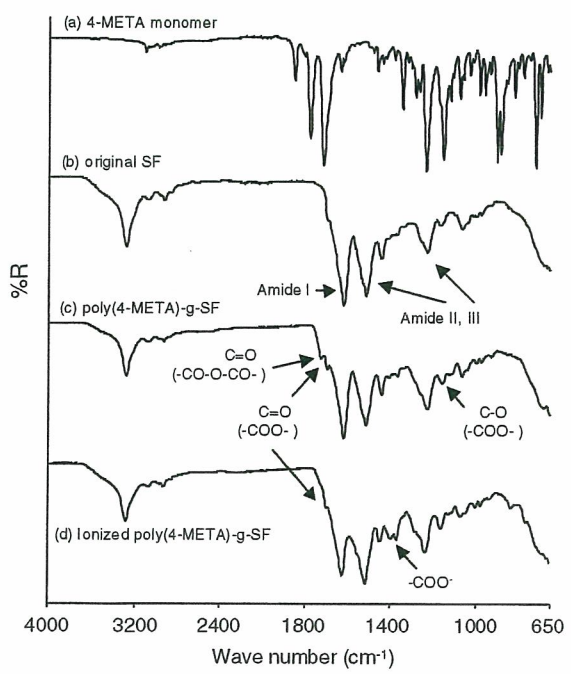

Figure 14. ATR FT-IR spectra of (a) 4-META monomer, (b) original SF, (c) poly(4-META)-grafted SF, and (d) ionized poly(4-META)-grafted SF.

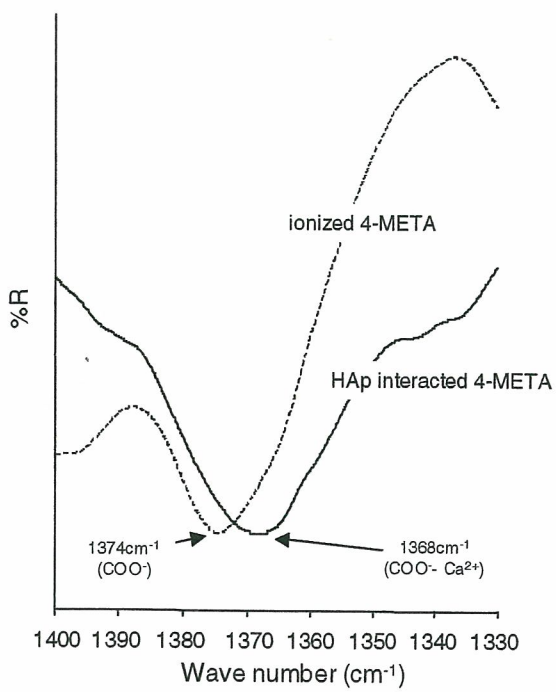

Figure 15. Difference FT-IR spectrum of diffuse reflectance which subtracts original HAp from HAp nanoparticles with ionized 4-META (solid line) and FT-IR spectrum of the ionized 4-META monomer (dashed line) at 1400–1330 cm^{-1}.

This synthetic procedure of the composite is outlined in Scheme 3.

By using the mixture of toluene and methanol, the HAp nanoparticles are equally dispersed in the medium and are adsorbed physically and dispersively on the SF surface because of the strong affinity between HAp and 4-META [8]. The SF, after ring-opening using a potassium hydroxide aqueous solution, moreover, has carboxylate groups on the surface. It is well known that the *a*-plane of HAp has a cationic surface which consists of Ca^{2+} ions [59]. It seems, therefore, that the *a*-plane of HAp was adsorbed on the SF covered with carboxylate groups. When the SF adsorbed with particles is washed in distilled water, K^+ ions are released from the SF, and $-COO^-$ in the ionized SF is coupled with the Ca^{2+} ions of HAp particles by ionic interaction due to the ionization tendency. In the series of our articles on the HAp/SF composite [18, 19, 21], the hydroxyl groups of HAp were needed to couple between the HAp nanoparticles and the SF substrate. In this synthetic method, however, these groups are not necessarily required, because the HAp particles are connected with the SF substrate by ionic interaction. By using 4-META, it is expected that not only HAp but also other inorganic compounds, such as β-tricalcium phosphate (β-TCP), can be adsorbed and connected on the SF fiber surface. In this way, HAp nonoparticles can be connected with modified SF under a nonheat condition, compared with the conventional way. This condition is useful when using non-heat-resistant biomedical material, such as polyethylene, as a polymer substrate for synthesizing the HAp/polymer composite.

3.4. Mechanical Properties

The tensile properties were measured by using TENSILON RTC-115 OA (ORIENTEC Co., Tokyo, Japan) at an elongation rate of 5 mm/min and 25°C. To determine the mechanical properties of the composite, a suture-like composite made of Kinsyu x Syowa (a variety of silk) was adopted. The unit of stress value was changed from *g/d* to *Pa* as shown by the following equations [63].

$A_0 = d/(9 \times 10^5 r)$,

A_0: cross-section area (cm^2),

d: denier (the experimental value = 97),

r: specific gravity (1.33 g/cm^3)

$S = P/(A_0 \times 10{-}^4)$

S: stress (Pa), P: experimental value of stress (N).

Data from the tensile test are presented as plus or minus standard deviation for the mean. Statistical comparisons were performed with the use of the Student's t-test and p values <0.01 were considered.

Figure 16 shows the tensile properties of three types of SF fiber (original SF, graftpolymer-grafted SF, and HAp/SF

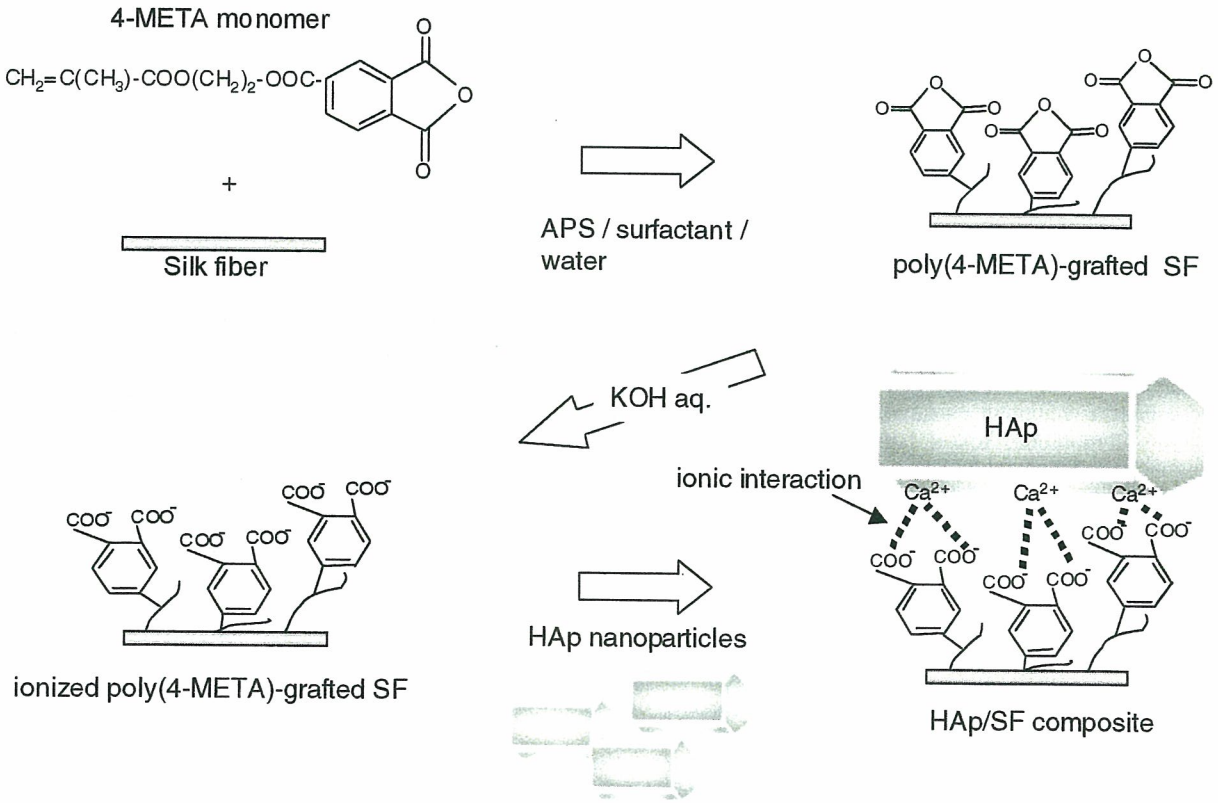

Scheme 3. Schematic presentation of the synthesis of the HAp/SF composite by ionic bonding.

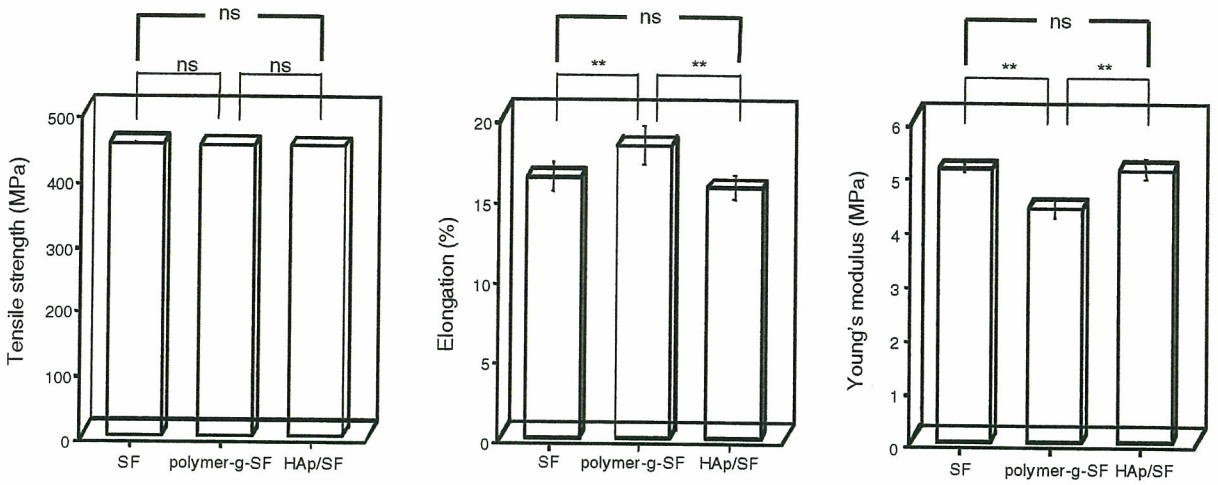

Figure 16. Mechanical properties of three types of SF fibers [original SF, (MOI-oxime)-grafted SF, and HAp/SF composite fiber]. Data were calculated as means of six-time determinations. Error bars represent standard deviations of six-time determinations. **means an existence of a significant difference ($P < 0.01$) between two samples.

composite). The tensile strengths, the elongation at break, and Young's modulus between the original SF and the HAp/SF composite were unchanged. Compared with the original SF and HAp/SF composite, the elongation at break of graftpolymer-grafted SF was somewhat higher but Young's modulus and thereof was somewhat lower, statistically. These results suggest that the difference of the elasticity may depend on the crystallinity on the surface. By means of the graft-polymerization on the SF, the crystallinity on the surface of SF decreases. The elasticity of polymer-grafted SF, therefore, decreases. After the coupling between HAp and the modified SF, it seems that the crystallinity is compensated by the covering with the inorganic substrate on the surface of SF and the elasticity of the HAp/SF composite is apparently equal to that of the original SF. These results show that this HAp/SF composite maintains flexibility equivalent to the original SF.

3.5. Cell Interaction

Mouse fibroblast cell lines of L929 cells were cultured in a complete α-minimum essential medium (α-MEM, Invitrogen Corporation, Tokyo, Japan), supplemented with heat-inactivated 10% fetal bovine serum (FBS, Gibco), 50 IU/ml of penicillin, 50 μg/ml of streptomycin, and 2.5 μg/ml of amphotericin B (ICN Biomedicals, Inc., Calif.). To detect cell adhesiveness on the samples, cell morphologies were observed by SEM. The L929 cells (1×10^5 cells/ml) were plated onto 24-well multiplates with fabric samples of 1.5 cm in diameter in an α-MEM with 10% FCS and incubated at 37°C for 24 h. As for the button-shaped samples, however, after the samples were immersed into 1.5-ml microtubes with 1.0 ml of the culture medium, an ultrasonic treatment was conducted via the tubes to remove gases from the gaps of the fibers for 1 min. The L929 cells were subsequently plated in the microtubes with the samples at 1×10^6 cells/tube in an α-MEM with 10% FCS and incubated at 37°C for 48 h. After being washed with phosphate-buffered saline [PBS(−)] three times, the samples were fixed with 2.5% buffered-glutaraldehyde for 20 min at 30°C. The cells were dehydrated with aqueous ethanol (30–100%) and 100% *n*-butanol for 5 min at room temperature step by step. The samples were lyophilized and coated with gold.

To evaluate the cell adhesiveness on the HAp-coated SF, the morphologies of L929 fibroblast cells incubated on sample fabrics or devices were observed by SEM. Figure 17 shows SEM observations of the surfaces of sample fabrics—gelatin-coated glass as a positive control (a), untreated SF (b), hydrolyzed poly(MPTS)-grafted SF (c) and HAp-coated SF (d)—incubated with L929 cells for 24 h. The cells hardly adhered on the hydrolyzed poly(MPTS)-grafted

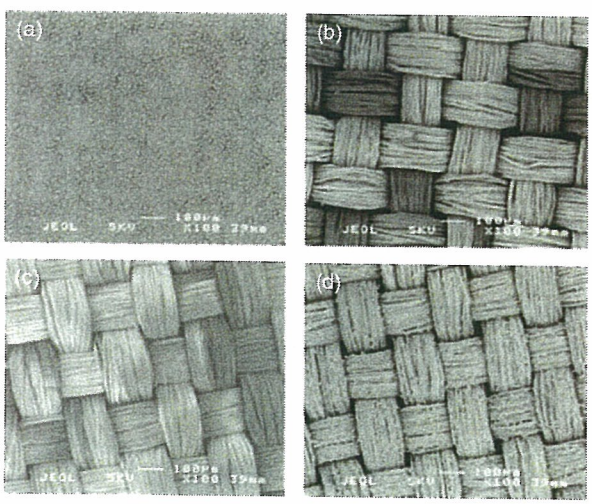

Figure 17. SEM photographs of cell morphologies on (a) gelatin-coated grass, (b) original SF fabric, (c) hydrolyzed poly(MPTS)-grafted SF fabric, and (d) calcined HAp nanoparticles covalently coated on an SF fabric. Reprinted with permission from [21], T. Furuzono et al., *J. Artif. Organs* 7, 137 (2004). © 2004, Springer.

SF as well as the untreated SF in Figure 17(b) and 17(c). Although it has been known that the initial cell adhesion on intact SF is actually not good [19, 20], the reason has not been thoroughly manifested. It is presumed to depend on high surface wettability due to containing many hydrophilic amino acid residues[17]—the hydroxyl group: Ser 10.63 mol%, Tyr 4.97 mol%, Thr 0.89 mol%; the carboxyl group: Asp 1.65 mol%, Glu 1.21 mol%; the amino groups: Lys 0.33 mol%, His 0.18 mol%, Arg 0.49 mol%—and peptide bonds without an arrangement of Arg-Gly-Asp (RGD) as a cell-adhesion molecule, or probably the existence of a microdomain structure [64] consisting of crystalline and amorphous regions attributed to an arrangement of $(Gly\text{-}Ala\text{-}Ser)_n$ and the other residues in SF. The cells indicated weak interaction with the hydrolyzed poly(MPTS)-grafted surface during the initial incubation period because of the surface hydrophilicity belonging to Si-OH moieties on Si-O-Si cross-linking networks produced by hydrolysis of the poly(MPTS)-grafted SF substrate demonstrated by ATR FT-IR analysis in Figure 11. Meanwhile, the cells adhered well on HAp-coated SF similarly to the previous reports [19, 20, 26] and as shown in Figure 17(d). The cross-sectional view of the composite with a cell stained shown in Figure 18. The needle-like microspikes from a cell incubated for 24 h were elongated to a calcined HAp nanoparticle chemical bonded on the polymer substrate. Cells, thus, favorably adhere only on the HAp surface of the composite but not on the dehydrated grafted-surface without HAp particles on the SF substrate. It is estimated that cell-adhesion proteins in serum, such as fibronectin, vitronectin, bFGF, and so, before cell adhesion, adsorb on a HAp surface much better than on an area of dehydrated graft-polymer (Scheme 4).

We previously reported that L929 cells restrictedly elongate their needle-like microspikes against an amino group-modified TiO_2 (TiO_2-NH_2) surface but that poly(acrylic acid(AAc))-grafted regions on the composite of TiO_2-NH_2 nanoparticles covalently linked onto a polyAAc-grafted silicone substrate [65]. A similar phenomenon takes place in the interface between a cell and a HAp composite on a nanoscaled HAp-coated SF substrate. That is to say, sintered HAp nanoparticles can provide bioactivity to a polymer substrate.

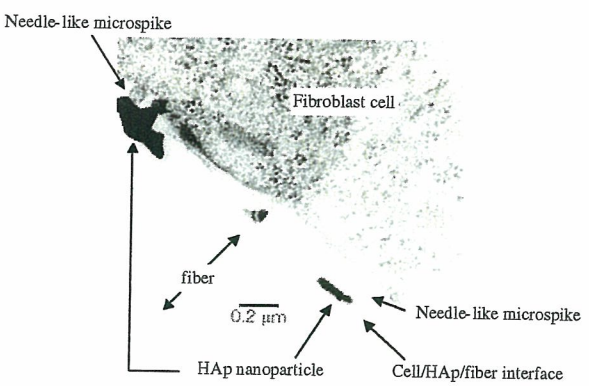

Figure 18. TEM micrograph of cross-sectional view of fiber/HAp/cell interface. The stained sample which is fibroblast incubated on HAp/SF for 24 h was cut by microtome. Reprinted with permission from [21], T. Furuzono et al., *J. Artif. Organs* 7, 137 (2004). © 2004, Springer.

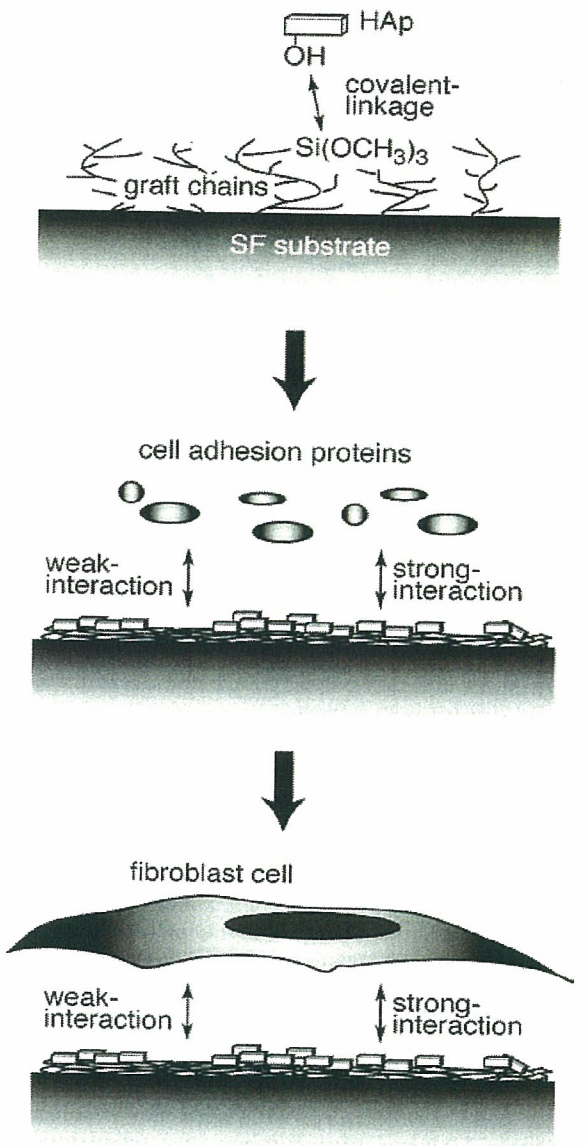

Scheme 4. Schematic presentations of the preparation of the composite and the expected mechanism of cell adhesion on calcined HAp nanoparticles coated SF. Reprinted with permission from [21], T. Furuzono et al., *J. Artif. Organs* 7, 137 (2004). © 2004, Springer.

4. FABRICATION OF MEDICAL DEVICES

4.1. A Percutaneous Device

A polymer substrate for a button form was molded using a silicone compound (KE153-U, Shin-Etsu Chemical Co. Ltd., Tokyo, Japan) to fix the pattern (Fig. 19). The internal diameter was based on the external diameter of a catheter for intravenous hyperalimentation (IVH). Silicone buttons covered with a silicone adhesive (TSE399, GE Toshiba Silicones Co., Ltd., Tokyo, Japan), which were then attached to a rotator on a motor that revolved at 450 rpm, by which HAp/SF fibers of about 100 mm in length thoroughly coated

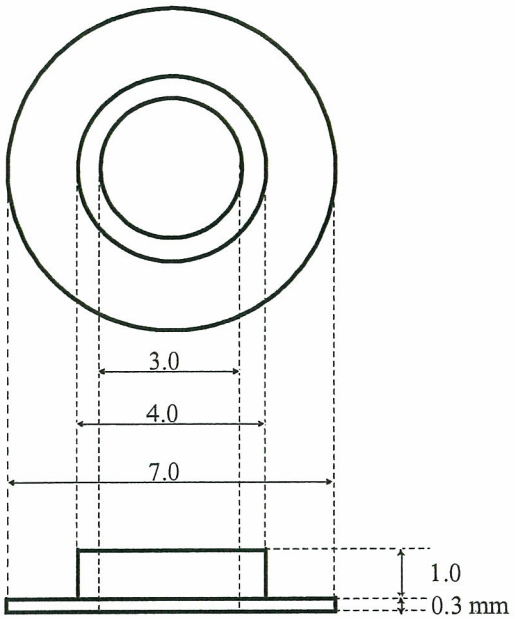

Figure 19. Design of a prototype model of a percutaneous button. Reprinted with permission from [21], T. Furuzono et al., *J. Artif. Organs* 7, 137 (2004). © 2004, Springer.

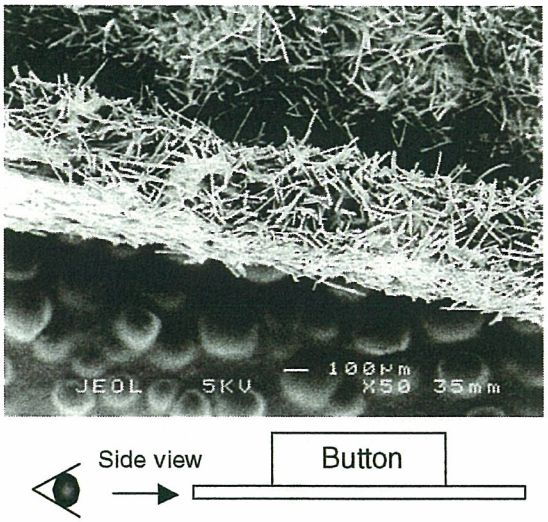

Figure 21. Magnified view of the edge of the button by SEM observation. Reprinted with permission from [21], T. Furuzono et al., *J. Artif. Organs* 7, 137 (2004). © 2004, Springer.

the buttons. The HAp/SF fiber-coated samples were heated at 120°C for 2 h in vacuum and were then washed in distilled water by using an ultrasonic generator for 3 min (output: 20 kHz, 35 W) to remove the fibers which adhered incompletely.

To fabricate a prototype for a percutaneous device, the HAp-coated SF fibers were transplanted onto a button-shaped substrate made of silicone via an adhesive agent. The weight ratio of three-dimensional coating consisting of composite fibers versus the total weight of the device was 14.3 ± 0.4 wt% ($n = 4$). The prototype of a button was fabricated by a silicone compound cast into a mold according to the illustration shown in Figure 19. The form was designed to install it a catheter for IVH whose outer diameter of tube showed 3.0 mm. Figure 20 shows the external appearances of the button allowing the catheter tube through. The device is white and very flexible. Figure 21 shows a magnified view of the edge of the button coated with HAp-modified SF fibers. The HAp-coated SF fibers of 100 μm in length were uniformly transplanted individually in random directions on the button.

A cell adhesion experiment using fibroblast cells was also conducted via the sample device. After incubation of untreated SF or HAp-coated SF buttons in a microtube for 48 h, the morphologies of the cells on both substrates were observed by SEM (Fig. 22). On HAp-coated SF buttons, the cells adhered and spread widely on the side surface. More spherical cells accumulated on other cells spread on the upper side of the button than on the side. This phenomenon shows that adhering cells accumulated in a multiple way on the substrate according to gravity in a three-dimensional incubation. However, few spherical cells were observed on untreated SF fibers transplanted on the button. These phenomena were equally consistent with the tendency of cell adhesiveness on the fabric samples. The three-dimensional composite is, therefore, useful as a cell

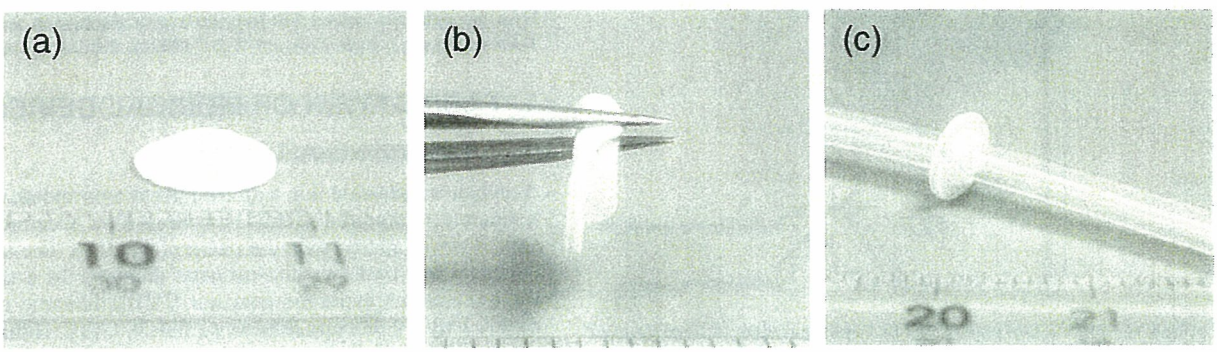

Figure 20. External views of the button prototype of a percutaneous device; (a) side view of the button, (b) flexibility of the button, and (c) a silicone tube installed in the button. Reprinted with permission from [21], T. Furuzono et al., *J. Artif. Organs* 7, 137 (2004). © 2004, Springer.

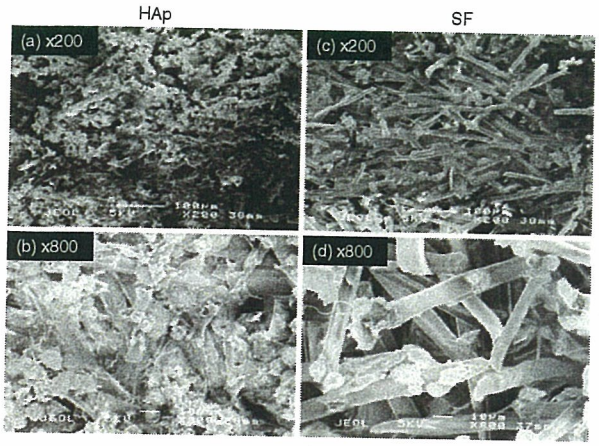

Figure 22. SEM photographs of cell morphologies on the upper views of the button made of (a, b) HAp-coated SF fibers and (c, d) untreated SF fibers. The magnification for (a, c) is ×200 and for (b, d), ×800. Reprinted with permission from [21], T. Furuzono et al., *J. Artif. Organs* 7, 137 (2004). © 2004, Springer.

scaffold. The percutaneous device was implanted in back of a rabbit for three months, according to the Guideline for Animal Experimentation National Cardiovascular Center. The skin tissue was adhered on the device without a gap between the tissue and the material surface, and severe inflammation and abscess was not observed from the external view (Fig. 23).

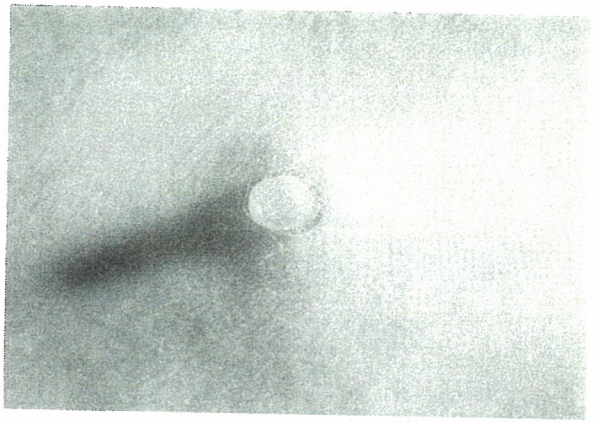

Figure 23. External view of the HAp-coated device percutaneously implanted into back of a rabbit for three months. The protruding substance is silicone tube, and HAp-coated percutaneous button is implanted just under the epidermis.

4.2. An Artificial Blood Vessel

We developed a novel inorganic-organic composite, consisting of calcined HAp nanoparticles chemically bonded on polymer substrate. HAp nanoparticles were covalently linked onto a poly(ethylene terephthalate) (PET) fabric substrate chemically modified by graft polymerization with MPTS for development of artificial blood vessel. Figure 24 shows SEM images of human umbilical vein endothelial cells (HUVEC) morphologies and fluorescence images of stained nuclei of HUVEC on sample substrates after 4 h of incubation. The initial interaction of HUVEC on substrates was evaluated after 4 h of incubation, according to several reports [66, 67]. In the SEM images, it seemed that many cells adhered on HAp/PET fabric as well as collagen-coated PET, while only a few cells adhered on the original fabric. The difference in the number of cells that adhered could not be distinguished by SEM observation, since HUVEC were flattened and spread over the substrate. The cells adhered were then stained by fluorescent dye and

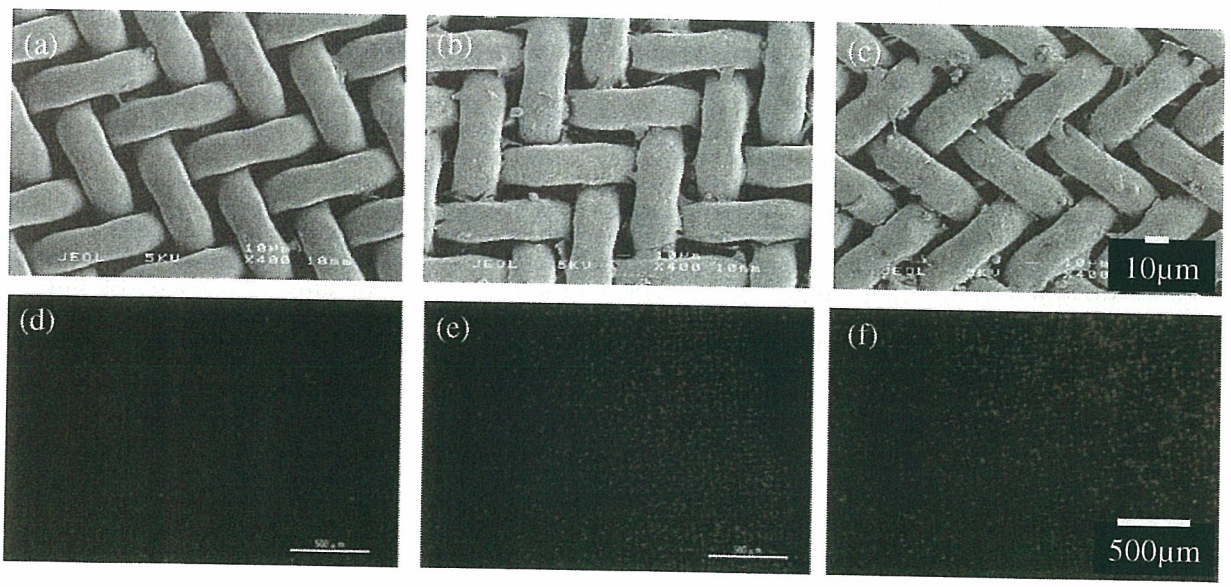

Figure 24. SEM and fluorescence photographs of HUVEC adhering on (a, d) original PET (b, d), collagen-coated PET, and (c, f) HAp/PET composite.

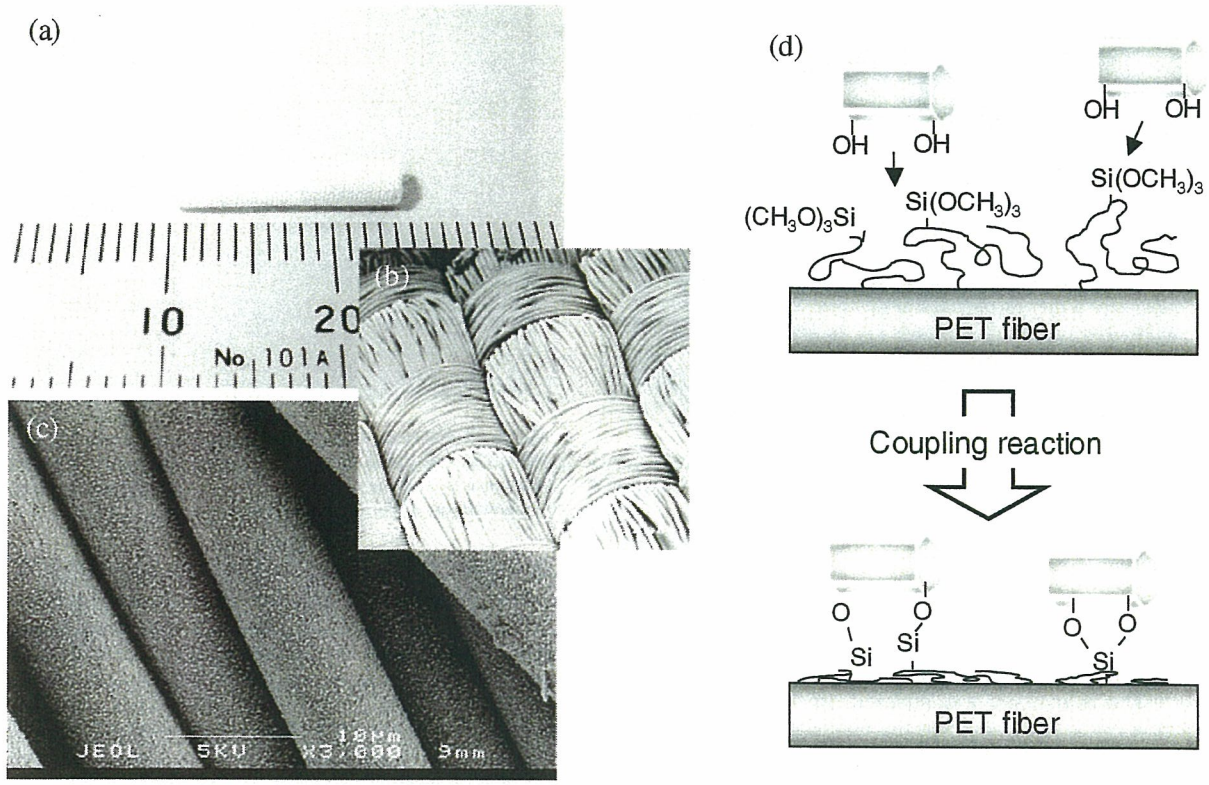

Figure 25. The images show prototype of an artificial blood vessel made of HAp/PET composite. (a) External view of the prototype. (b, c) Lower and higher magnification of SEM images of HAp/PET fibers of inside of the prototype. (d) Schematic presentation of the reaction process of calcined HAp nanoparticles covalently coated on a PET fiber.

observed by a fluorescence microscope. It was found that the number of cells adhered on HAp/PET was qualitatively the same as that of collagen-coated PET, although the cells seldom adhered on the original PET for such a short period of incubation. This phenomenon can be explained because cell adhesion proteins such as fibronectin or vitronectin in a culture medium may be favorably adsorbed on the HAp surface [22]. In other words, calcined HAp coating on popular biomedical substrates is effective to obtain the affinity of cells without using biological scaffold proteins such as collagen or gelatin. The HAp/PET composite is very meaningful for biological safety in medical fields today when the danger of BSE infection by using proteins derived from a bovine animal is trumpeted loudly. A prototype of artificial blood vessel made of the HAp/PET composite was fabricated (Fig. 25). The calcined HAp nanoparticles were thoroughly coated on PET fibers of inside and outside of an artificial blood vessel. The effect of HAp nanocrystals on it through animal implantation experiments *in vivo* are under evaluation.

5. CONCLUSIONS

Well-crystallized and calcined HAp nanoparticles with free impurities were synthesized through the modified emulsion process. The morphology and size of the HAp nanoparticles were drastically changed by altering the reaction temperature. Calcined HAp nanoparticles with spherical, or rodlike, morphologies well-dispersed in a liquid media were also successfully prepared by calcinations using an antisintering agent interspersed between or surrounding the particles, followed by removal of the agent. The inorganic-organic composite, consisting of calcined HAp nanoparticles and polymer substrates, were prepared through chemical bonding, such as covalent or ionic bonding. The elasticity of the composite was not change compared with the original polymer substrates. The cell-adhesion test shows that the HAp/polymer substrate improves bioactivity compared with original substrates. Cells were also able to penetrate into the gaps between the inorganic-organic composite in a three-dimensional tangle. A percutaneous device and an artificial blood vessel were fabricated from the HAp composite polymer fibers have been examined by animal implant experiments.

Preparation of composites consisting of calcined HAp nanoparticles and polymer substrates, for examples, mixture, *in situ* or nanochemical bonding methods, is necessary for nanoscaled observation from the points of view of the bulk structures, surface properties, and biological interactions. For our composite, especially, the size, coverage ratio, or strength of chemical bonding of sintered HAp nanoparticles are assumed to be important for interactions with biomolecules such as proteins, cells, and tissues to develop medical devices. This composite material is expected to

establish a novel concept for fabrication of an inorganic-organic composite as biocompatible materials for hard and soft tissue.

ACKNOWLEDGMENTS

The authors are grateful to Dr. Junzo Tanaka, Biomaterials Center, National Institute for Materials Science, and Prof. Akio Kisida, Institute of Biomaterials and Bioengineering, Tokyo Medical and Dental University, for their helpful advices and supports. A series of the study about the development of the nanocomposite was financially supported in part by research programs of Japan Science and Technology Corporation (JST)—CREST, PRESTO, and Innovation Plaza Osaka—and promoting projects on Comprehensive Research on Cardiovascular Diseases.

REFERENCES

1. H. Aoki, "Medical Applications of Hydroxyapatite." Ishiyaku, EuroAmerica, Tokyo, 1994.
2. V. Midy, C. Rey, E. Bres, and M. Dard, *J. Biomed. Mater. Res.* 41, 405 (1998).
3. C. C. Veheyen, J. R. de Wijn, C. A. van Blitterswijk, K. de Groot, and P. M. Rozing, *J. Biomed. Mater. Res.* 27, 433 (1993).
4. M. Wang, R. Joseph, and W. Bonfield, *Biomaterials* 19, 2357 (1998).
5. S. I. Stupp and G. W. Ciegler, *J. Biomed. Mater. Res.* 26, 169 (1992).
6. K. Kato, Y. Eika, and Y. Ikada, *J. Biomed. Mater. Res.* 32, 687 (1996).
7. M. Kikuchi, S. Itoh, S. Ichinose, K. Shinomiya, and J. Tanaka, *Biomaterials* 22, 1705 (2001).
8. M. C. Chang, T. Ikoma, M. Kikuchi, and J. Tanaka, *J. Mater. Sci. Mater. Med.* 13, 993 (2002).
9. S. Ito, M. Kikuchi, Y. Koyama, K. Takakuda, K. Shinomiya, and J. Tanaka, *Cell Transplant.* 13, 451 (2004).
10. H. M. Kim, T. Himeno, T. Kokubo, and T. Nakamura, *Biomaterials* 26, 4366 (2005).
11. G. J. Liu, F. Miyaji, T. Kokubo, H. Takadama, T. Nakamura, and A. Murakami, *J. Mater. Sci. Mater. Med.* 9, 61 (1998).
12. T. Taguchi, A. Kishida, and M. Akashi, *Chem. Lett.* 711 (1998).
13. T. Furuzono, T. Taguchi, A. Kishida, M. Akashi, and Y. Tamada, *J. Biomed. Mater. Res.* 50, 344 (2000).
14. T. Taguchi, Y. Muraoka, H. Matsuyama, A. Kishida, and M. Akashi, *Biomaterials* 22, 53 (2001).
15. K. de Groot, R. Geesink, C. P. A. T. Klein, and P. Serekian, *J. Biomed. Mater. Res.* 21, 1375 (1987).
16. T. Furuzono, D. Walsh, K. Sato, K. Sonoda, and J. Tanaka, *J. Mater. Sci. Lett.* 20, 111 (2001).
17. K. Sonoda, T. Furuzono, D. Walsh, K. Sato, and J. Tanaka, *Solid State Ionics* 151, 321 (2002).
18. T. Furuzono, A. Kishida, and J. Tanaka, *J. Mater. Sci. Mater. Med.* 15, 19 (2004).
19. A. Korematsu, T. Furuzono, S. Yasuda, J. Tanaka, and A. Kishida, *J. Mater. Sci.* 39, 3221 (2004).
20. A. Korematsu, T. Furuzono, S. Yasuda, J. Tanaka, and A. Kishida, *J. Mater. Sci. Mater. Med.* 16, 67 (2005).
21. T. Furuzono, S. Yasuda, T. Kimura, Si. Kyotani, J. Tanaka, and A. Kishida, *J. Artif. Organs* 7, 137 (2004).
22. T. Furuzno, M. Masuda, M. Okada, S. Yasuda, H. Kadono, R. Tanaka, and K. Miyatake, *ASAIO J.* 7, 137 (2004).
23. M. Taniguchi, H. Takeyama, I. Mizuno, N. Shinagawa, J. Yura, N. Yoshiyama, and H. Aoki, *Jpn. J. Artif. Organs* 20, 460 (1991).
24. P. M. Zabetakis, C. M. Cotell, D. B. Chrisery, and R. C. Auyeung, *ASAIO J.* 40, M896 (1994).
25. T. Furuzono, K. Sonoda, and J. Tanaka, *J. Biomed. Mater. Res.* 56, 9 (2001).
26. T. Furusono, P. Wang, A. Korematsu, K. Miyazaki, M. Oido-Mori, Y. Kowashi, K. Ohura, J. Tanaka, and A. Kishida, *J. Biomed. Mater. Res. B: Appl. Biomater.* 65B, 217 (2003).
27. M. Jarcho, C. H. Bolen, M. B. Thomas, J. Bobick, J. F. Kay, and R. H. Doremus, *J. Mater. Sci.* 11, 2027 (1976).
28. H. K. Schmidt, *Mol. Cryst. Liq. Cryst.* 353, 165 (2000).
29. B. L. Cushing, V. L. Kolesnichenko, and C. J. O'Connor, *Chem. Rev.* 104, 3893 (2004).
30. S. Somiya, K. Ioku, and M. Yoshimura, *Mater. Sci. Forum* 34–36, 371 (1988).
31. M. Yoshimura, H. Suda, K. Okamoto, and K. Ioku, *J. Mater. Sci.* 29, 3399 (1994).
32. A. D. Papargyris, A. I. Botis, and S. A. Papargyri, *Key Eng. Mater.* 206–213, 83 (2002).
33. Y. Masuda, K. Matsubara, and S. Sakka, *J. Ceram. Sci. Jpn.* 98, 1226 (1990).
34. C. Sanchez and J. Livage, *New J. Chem.* 14, 513 (1990).
35. H. K. Schmidt, E. Geiter, M. Mennig, H. Krug, C. Becker, and R. P. Winkler, *J. Sol.-Gel Sci. Tech.* 13, 397 (1998).
36. G. K. Lim, J. Wang, and S. C. Ng, L. M. Gan, *Mater. Lett.* 28, 431 (1996).
37. G. Guo, Y. Sun, Z. Wang, and H. Guo, *Ceram. Int.* 31, 869 (2005).
38. Y. Wu and S. Bose, *Langmuir* 21, 3232 (2005).
39. G. K. Lim, J. Wang, S. C. Ng, and L. M. Gan, *Mater. Lett.* 28, 431 (1996).
40. W. H. Emerson and E. E. Fisher, *Arch. Oral Biol.* 7, 671 (1962).
41. R. Z. LeGeros, in "Calcium Phosphate in Oral biology and Medicine" (H. M. Hyers, Ed.). Karger, New York, 1991.
42. L. Qi, J. Ma, M. Cheng, and Z. Zhao, *J. Mater. Sci. Lett.* 16, 1779 (1997).
43. G. K. Lim, J. Wang, S. C. Ng, and L. M. Gan, *J. Mater. Chem.* 9, 1635 (1999).
44. S. Mann, J. Didymus, N. P. Sanderson, B. R. Heywood, and E. J. A. Samper, *J. Chem. Soc. Faraday Trans.* 86, 1873 (1990).
45. J. Frenkel, *J. Phys. USSR* 9, 385 (1945).
46. G. C. Kuczynski, *Trans. AIME* 185, 169 (1949).
47. J. E. Barralet, S. M. Best, and W. Bonfield, *J. Mat. Sci. Mater. Med.* 11, 719 (2000).
48. E. Landi, A. Tampieri, G. Celotti, and S. Sprio, *J. Eur. Ceram. Soc.* 20, 2377 (2000).
49. D. Bernache-Assollant, A. Ababoua, E. Championa, and M. Heughebaertb, *J. Eur. Ceram. Soc.* 23, 229 (2003).
50. J. E. Carless and A. A. Foster, *J. Pharmaceut. Pharmacol.* 18, 697 (1966).
51. M. Wei, A. J. Ruys, B. K. Milthorpe, and C. C. Sorrell, *J. Biomed. Mater. Res.* 45, 11 (1999).
52. K. Nishizawa, M. Toriyama, T. Suzuki, Y. Kawamoto, Y. Yokogawa, and F. Nishizawa, *Chem. Soc. Jpn.* 1, 63 (1995).
53. R. Labella, M. Braden, and S. Deb, *Biomaterials* 15, 1197 (1994).
54. A. M. P. Dupraz, J. R. de Wijn, S. A. T. vd de Meer, and K. de Groot, *J. Biomed. Mater. Res.* 30, 231 (1996).
55. Q. Kiu, J. R. de Wijn, K. de Groot, and C. A. van Blitterswijk, *Biomaterials* 19, 1067 (1998).
56. P. E. Cranley, *Polym. Sci. Technol.* 29, 765 (1984).
57. T. Furuzono, K. Ishihara, N. Nakabayashi, and Y. Tamada, *J. Appl. Polym. Sci.* 73, 2541 (1999).
58. Q. Liu, J. R. de Wijn, and C. A. van Blitterswijk, *J. Biomed. Mater. Res.* 40, 257 (1998).
59. T. Kawasaki, *J. Chromatogr.* 544, 147 (1991).
60. Y. Abe, M. Kiyomura, K. Nagata, and N. Nakabayashi, *J. Jpn. Dent. Mater.* 5, 310 (1986).

61. M. Kikuchi, Y. Suetsugu, J. Tanaka, S. Itoh, S. Ichinose, K. Shinomiya, Y. Hiraoka, Y. Mandai, and S. Nakatani, in "Bioceramics, Proceedings of the 12th International Symposium on Ceramics in Medicine" (H. Ohgushi, G. W. Hastings, and T. Yoshikawa, Eds.), Vol. 12, p. 393. World Scientific Publishing, Singapore, 1999.
62. J. Tanaka and M. Kikuchi, *Ceram. Jpn.* 34, 543 (1999).
63. Nippon-Sen'I-Kikai-Gakkai, eds., Sangyoyo-sen'I-sizai Handbook, Tokyo, 1979, p. 8.
64. N. Yui, Y. Suzuki, H. Mori, and N. Okano, in "Surface Science of Crystalline Polymers" (N. Yui and M. Terano, Eds.), p. 121, Kodansha Scientific, Tokyo, 1996.
65. T. Furuzono, M. Iwasaki, S. Yasuda, A. Korematsu, T. Yoshioka, S. Ito, and A. Kishida, *J. Mater. Sci. Lett.* 32, 1737 (2003).
66. P. Hamerli, T. Weigel, T. Groth, and D. Paul, *Biomaterials* 24, 3989 (2003).
67. S. P. Massia and J. A. Hubbell, *J. Biomed. Mater. Res.* 25, 223 (1991).

大動脈瘤・大動脈解離診療のコツと落とし穴

編集● 田林 晄一
栗林 幸夫

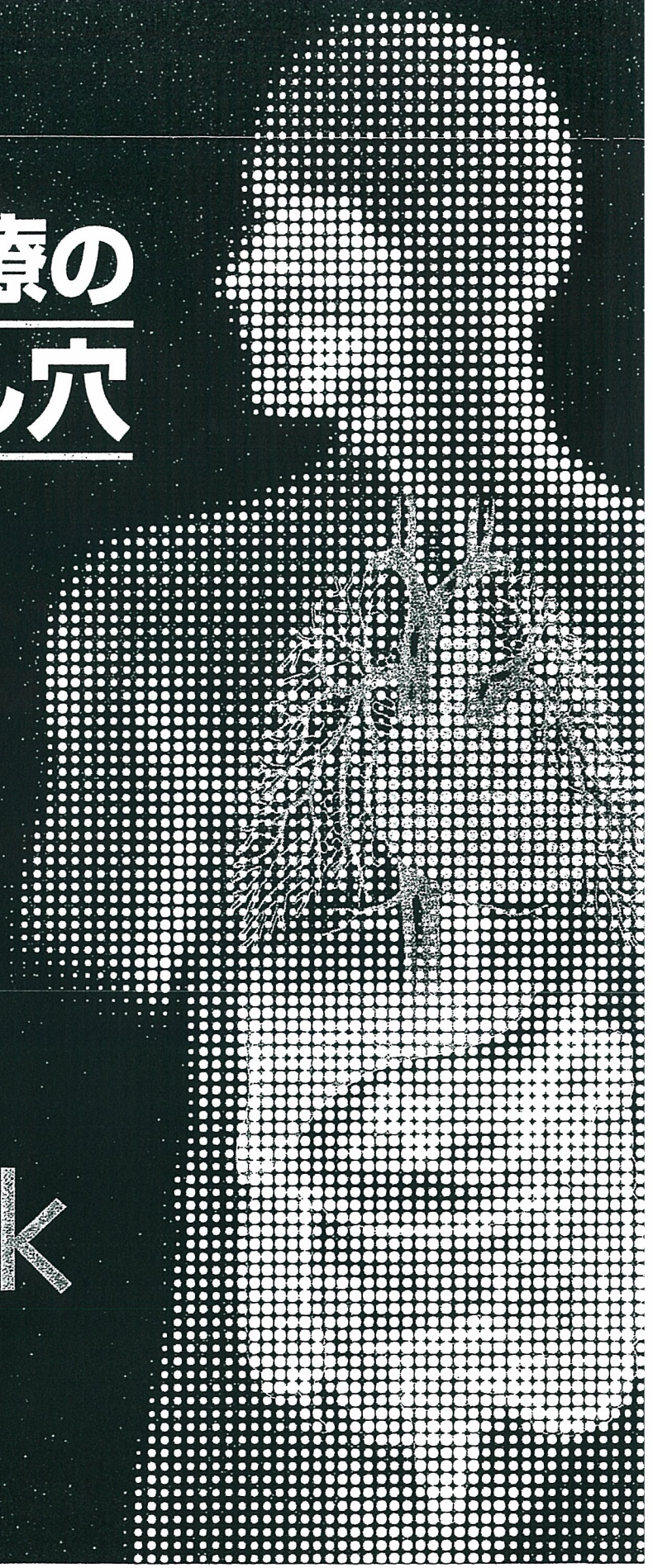

Pitfalls & Knack

中山書店

腹部大動脈瘤ステントグラフト治療において重要な側副血行のCT診断

田中 良一（国立循環器病センター）

ステントグラフトだけでは制御できない問題の一つにtype IIエンドリークがある

腹部大動脈瘤のステントグラフト治療は低侵襲性であることより，重症合併症を有する症例において有効な治療法だが，ステントグラフトだけでは制御できない問題の一つに主要分枝からの逆行性血流によるいわゆるtype IIエンドリークがある．また，瘤の形態によっては，内腸骨動脈など分枝の閉塞を必要とすることもあり，その分枝末梢に存在する組織への血流供給について検討しておくことも重要である．ここでは，CTにおいて判定できる側副血行のうち，腹部大動脈瘤ステントグラフト治療に関連すると思われるものを提示する．

大動脈関連の側副血行では腰動脈と下腸間膜動脈に注意

大動脈に関連した側副血行では，ステントグラフトtype IIエンドリークを起らす血管として腰動脈および下腸間膜動脈が重要である．いずれの血管も動脈硬化や瘤に関連する壁在血栓の影響で術前に閉塞していることもあるが，開存している場合はその大きさや他の血管との末梢吻合に留意する必要がある．腰動脈は他のレベルの腰動脈や内腸骨動脈の分枝である腸腰動脈と吻合することがあり（❶），下腸間膜動脈は上腸間膜動脈と

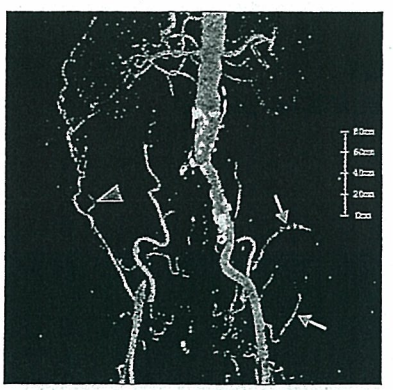

❶ 腰動脈・大腿動脈から内腸骨動脈分枝への吻合
造影CTアンギオグラフィ（最大値投影法）正面像．閉塞性動脈疾患により右総腸骨動脈および外腸骨動脈が閉塞．また，左内腸骨動脈も閉塞している．右では腰動脈から腸腰動脈への側副路（矢頭）が発達し，腰動脈から腸骨回旋動脈への側副路もみられる．左では内側および外側大腿回旋動脈から下殿動脈，上殿動脈への側副路（矢印）がみられる．また，本例では両側内胸動脈と吻合する下腹壁動脈も側副路として発達しているが，これらは下肢血流には関連するが，エンドリークに関与する側副路ではない．

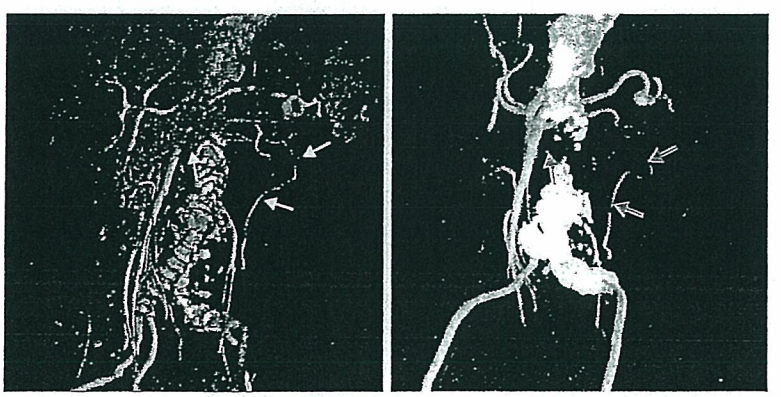

❷ 上腸間膜動脈から下腸間膜動脈への側副路
本例はステントグラフト留置後にエンドリークが残存した症例である．側副路をみやすいように大動脈の一部を削除している．上腸間膜動脈から下腸間膜動脈への側副路がみられる（矢印）．三次元再構成でわかりやすい術後の拡張した側副路を表示しているが，本例ではステントグラフト術前より横断像では上腸間膜動脈と下腸間膜動脈の連続がみられていた．

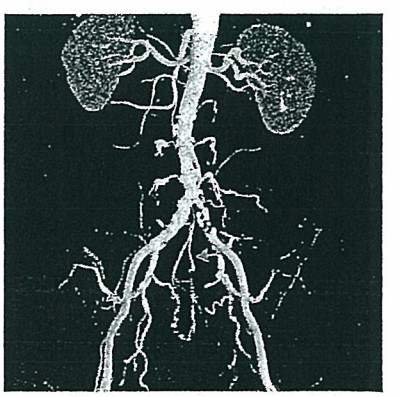

❸ 内腸骨動脈分枝どうしおよび正中仙骨動脈の吻合
左総腸骨動脈閉塞症例．右内腸骨動脈から左内腸骨動脈へ吻合がみられる．また，正中仙骨動脈も側副路として発達している（矢印）．

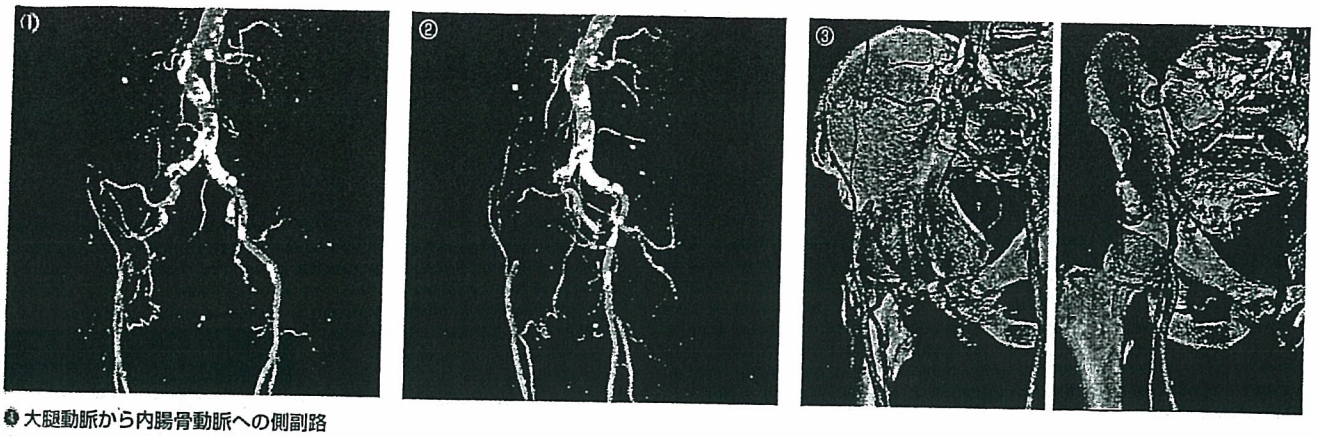

❶大腿動脈から内腸骨動脈への側副路
①正面像．右外腸骨動脈閉塞の症例の最大値投影法．内腸骨動脈から閉鎖動脈および外陰部動脈を介し，右総大腿動脈に連続する側副路を認める．本例では下肢への側副路として内腸骨動脈から大腿動脈方向へ血流があると考えられるが，内腸骨動脈閉塞の場合は逆流する側副路として重要である．
②左前斜位像．斜位にて側副路の連続が明瞭となっている．
③ボリュームレンダリング像．側副路と骨との関係がわかる．閉鎖孔を通る閉鎖動脈が拡張していることがわかる．

中結腸動脈を介して潜在的な側副路を形成する（❷）．これらは三次元画像では判定が難しい場合もあるが，二次元画像をたんねんに追跡すると連続性の有無を確認できる．開存している血管であるにもかかわらず，術前にこれらの側副血行となる血管との連続性を確認できる場合は，術後のエンドリーク発生に特に注意すべきであろう．また，正中仙骨動脈は内腸骨動脈の分枝である外側仙骨動脈と吻合することがある（❸）．

腸骨動脈関連の側副血行では治療前の側副路評価が重要

ステントグラフト治療の際，瘤の形態によっては内腸骨動脈の塞栓を行う必要がある．経験的に内腸骨動脈へは豊富な側副血行があることは認識されており，塞栓が問題となることは必ずしも多くない．しかし，瘤に伴って閉塞性動脈疾患を合併し塞栓すべき内腸骨動脈と反対側の内腸骨動脈に高度の狭窄や閉塞が存在する場合，腸管虚血の合併症を考慮しなくてはならず治療前の側副路評価は重要となる．通常，内腸骨動脈およびその分枝へは対側の内腸骨動脈分枝である外側仙骨動脈，子宮動脈，中直腸動脈，下膀胱動脈，閉鎖動脈内陰部動脈が吻合し連続する（❸）が，そのほかに腰動脈，正中仙骨動脈が側副路として有名である．ただし，これらの動脈は上記のようなステントグラフト留置の場合には有効な側副路としては機能しないことがあり，その場合は外陰部動脈から閉鎖動脈そして内腸骨動脈へ連続する側副路の発達は重要である（❹）．また，肋間動脈や肋下動脈からの側副路が吻合することもあり，これらの連続性を確認しておく必要がある．さらに，内側および外側大腿回旋動脈から下殿動脈，上殿動脈への側副路も評価が必要である．これらの評価においても三次元画像は必ずしも適当ではなく二次元画像をたんねんに追跡することが重要だが，十分に発達した側副路は丁寧に作成された三次元画像で評価が可能な場合もある（❶）．

臨床放射線 51巻11号（10月臨時増刊号）

Interventional Radiologyのコツ

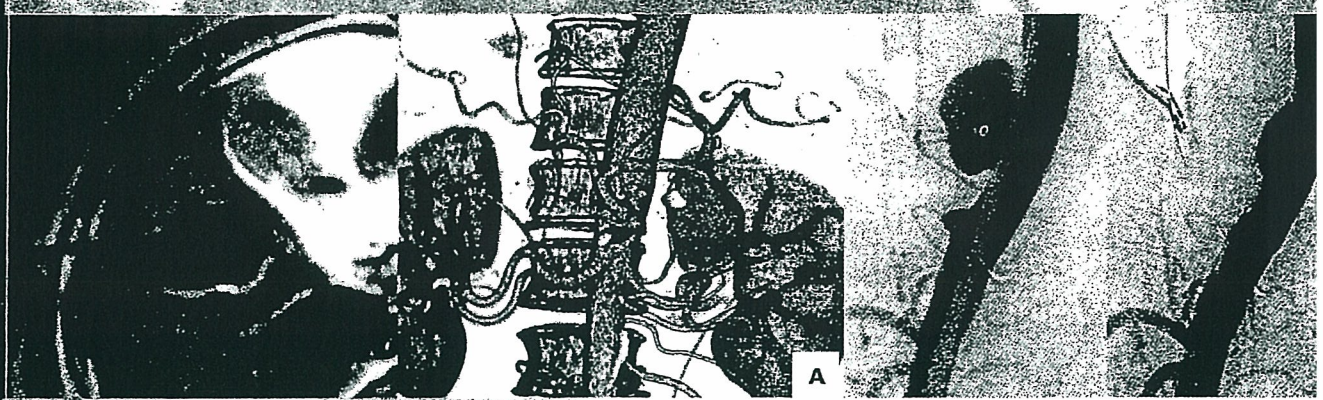

●編集：臨床放射線編集委員会

金原出版株式会社

［臨放 Jpn J Clin Radiol］
2006年10月31日発行

骨盤下肢動脈の PTA/ステント

田中良一*

はじめに

骨盤から下肢動脈における閉塞性動脈疾患に対するPTAおよびステントはデバイスの発達とともに適応が広がり，一般的な治療法として行われるようになってきている。一方で，血管を詰める操作ではなく，広げて血流を確保する操作である点が一般的なinterventional radiology（IVR）とは異なる点であり，治療戦略の立て方も異なってくる。本稿では骨盤下肢動脈のPTAとステントについて領域ごとの治療成績の違いから，治療戦略の立て方およびデバイス選択や治療時のコツについて述べる。

❶ 骨盤下肢動脈におけるIVRの成績

末梢血管の閉塞性動脈疾患においてはTrans Atlantic Inter-Society Consensus（TASC）によるconsensus paperが2000年に出されており[1]，この内容はインターネットでも確認できる，（URL：www.tasc-pad.org）。これは1999年までのデータをまとめたものであり，現時点ではやや内容が古くなっているが，閉塞性動脈疾患における標準的な教科書であるといってもよいと思われる。（内容をアップデートしたEssential TASCでは2000年以降のデータを踏まえ，IVRの適応もやや拡大される様子である。）

腸骨動脈領域においては，ステント（図1）を用いることにより良好な成績を示すことが示されており[2-4]，TASC C，Dのような長区域病変であっても治療成績が良好であることが示されている[5]。一方で，大腿動脈においては様々な工夫がなされている[6-9]が，腸骨動脈と比較して治療成績は必ずしも満足いくものとはいえない。また，同領域におけるステント挿入は現在のところ明確な治療成績の改善をもたらすものではなく，また，大腿動脈の可動性に基づく遠隔期におけるステント破損の問題があり，ステント破損に伴う再狭窄のみならず，低い発生頻度ではあるようだが血管損傷による仮性動脈瘤形成などの問題点もある。この領域においては，Boliaら[10][11]によってsubintimal angioplastyが提唱されてから，長区域閉塞に対する血管形成術が盛んに行われるようになった歴史があるが，原法はステントを使用せずに開存を得るための方法であった。しかし，昨今，ステントが多用されるようになり，十分な拡張が行われないままステントが使用されていることは憂慮すべきであろう。

下腿においては重症虚血趾に対する治療が主となる[12-16]が，非常に状態が悪い血管に対して治療を行うこととなり，閉塞病変に対する治療が必要となる事も多い。治療が不成功の場合，趾切断に至るリスクも十分にあることを念頭におく必要がある。

❷ 部位別の治療の特徴とコツ

1）腸骨動脈

腸骨動脈は国際的にもIVR治療のコンセンサスが得られている領域であり，ステントを含めデバイスの選択枝も最も多い領域である。以前は血管造影ですべて判断せざるを得なかったが，現在では超音波検査，MRI，CTと様々なモダリ

* 岩手医科大学放射線科
〔索引用語：PTA，ステント，下肢動脈〕

ティを駆使して事前に情報を収集できる。まず，治療対象となる病変の局在と性状を把握することが大切で，病変の石灰化の有無，病変部および前後の血管におけるremodelingの有無が重要である。狭窄性病変を有する部にしばしば厚いプラークを伴う瘤状拡張がみられる場合もあり，このような症例においては腹部大動脈瘤などを合併する事も多い。また，内腸骨動脈の分岐や開存の有無，側副路の状態を把握しておく事も重要である。腸骨動脈において内腸骨動脈近傍に病変が存在する場合，内腸骨動脈をまたぐようにステントを挿入せざるを得ない症例も多い。多くの場合，臨床的に問題となることはないが，反対側の内腸骨動脈の開存の有無や腰動脈などの側副路となりうる血管の状態を把握しておくことは重要である。事前の情報収集で最も重要なことはアクセスルートを決めることであるが，我々はできるだけ病変と同側で近い位置からの治療を原則としている。これは治療の難易度を下げ，より安全にかつ短時間に治療を行うために重要なポイントと考える。ただし，総大腿動脈の拍動を触れにくいため，穿刺には慣れも必要である。同側からのアプローチだけでなく，反対側からのアプローチも行い，穿刺の際には反対側から挿入したカテーテルから造影を行って血管の走行を確かめて穿刺する方法も重要であろう。

腸骨動脈の場合にはステント治療の長期成績が良好であるため，ステント挿入になることが多いが，プラーク量が少ない非常に限局した病変の場合にはバルーンPTAだけで十分な場合もある。バルーンのみで治療する際には，前後の対象血管径と同じかやや大きめのバルーンを使用する。原理上，限局解離が起こるが，小さな解離であれば低圧（1～3気圧）で長時間（3～5分）の拡張を行うことで十分に拡張が得られる事も多い。使用するバルーンは好みにも左右されるが，我々はセミ・コンプライアント・バルーンを使用している。セミ・コンプライアント・バルーンの場合は，定格のバルーン径に広がるための圧（nominal pressure）があり，これより加圧すると若干ではあるがバルーン径を大きくすることもできる。ただし，nominal pressureとrated burst pressureの差が大きいのはバルーン径の変化量も大きく，しばしば病変を広げたい場合に有用であるが，しばしばバルーンの両端のほうが大きく拡張し，病変部より健常部を広げてしまう結果となる事もあるため注意が必要である。また，バルーンはステント留置における前拡張や後拡張においても重要である。遠位塞栓に関連して前拡張には様々な議論があるが，我々はステント挿入を前提とした場合，4～5mm径のバルーンで前拡張を行っている。過拡張は遠位塞栓の危険性を増すため避けるべきだが，ステント挿入時の不完全拡張や後拡張バルーンの挿入困難が生じないようにする目的がある。

腸骨動脈においてステントは重要なデバイスであるが，ステントにはバルーン拡張型ステントと自己拡張型ステントがある。本邦ではバルーン拡張型ステントで血管用デバイスとして認可を受けているものはPalmaz stent（図1A）のみである。Palmaz stentはスリットが入ったステンレスのチューブがバルーンに載せられた形をしており，radial forceが強く，留置時の位置決めを行いやすい特徴がある。しかし，いったん外圧などで潰れると元に戻らないことや，血管を直線的に伸ばすため外圧がかかりやすい場所や屈曲部には使いにくい。挿入時にはステントの脱落を防ぐため，病変部を超えてシースを挿入し，シースの中でステントを進めて病変部まで持ってきた後，シースを引いてステントを露出させるようにする必要がある。シースを挿入できない場合は事前に十分に血管を広げておき，途中でステントが病変に引っかかって脱落しないように注意する必要がある。

自己拡張型ステントはバルーン拡張型ステントと異なり，自己拡張力があるため，外圧による変形に強い特徴がある。ステントの形態により，拡張力や留置時のステント短縮が異なるが，これらの特徴から考えて大きく二つの製品群に分けられると考える。ひとつはWallstent（図1B）でこれは網の目状に金属ワイヤを編んだもので，拡張しながらステントが短縮する特徴を

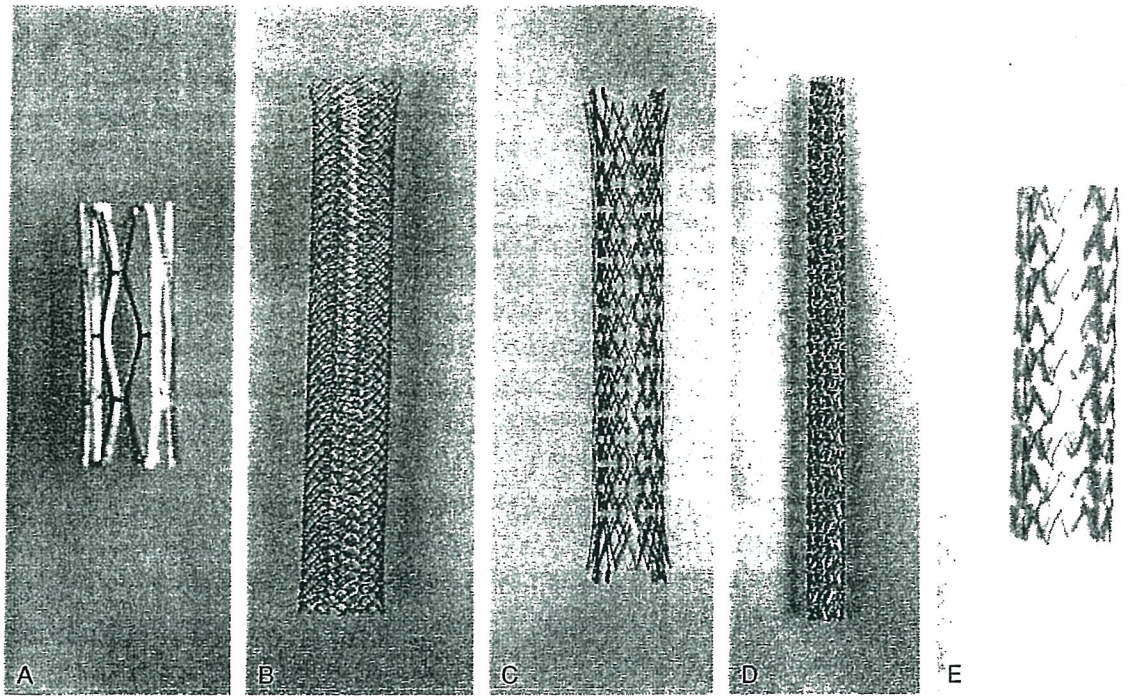

図1　本邦で保険認可されている各種血管用ステント
A　Palmaz stent　唯一のballoon expandable stentである。B　Wallstent　写真はEasy Wallstentである　C　Luminexx
D　SMART er　E　SelfX

持つ。短縮が顕著であるため，ステントの選択や位置決めがややむずかしく，挿入時のテクニック（プッシュ・イン）を要する事もあるがステントメッシュが細かく，ステント内へのプラーク突出をみることが少ないのが特徴である。また，展開途中でもシース内に再収納（リシース）して位置決めをやり直すことができるのも特徴のひとつである。もう一つの製品群はLuminexx（図1C）やSMART stent（図1D）でナイチノールをレーザーカットで形成したものである。留置時の短縮が少なく厳密な留置が可能だが，リシースはできないため，展開前の位置決めと展開時のズレを起こさないような工夫が必要である。これらの最近の製品群にはコントロールハンドルと呼ばれる展開用ツールが手元についており，厳密な位置決めをやりやすくする工夫がみられる。Luminexxでは規格に短いステントがあるのが魅力ではあるが，短いステントを展開しようとする際には，ステントが飛び出して位置がずれないように，あまりゆっくりと展開せずにスピーディに展開するのがコツである。LuminexxとSMART stentの大きな違いはブリッジの本数とstentのオープンエリアの広さにある。Luminexxではステントを長軸方向で接合するブリッジの本数が少ないため，ステント自体の柔軟性を増しているが，ひとつひとつのベンド部分の長さが長いため，各々のベンドのエッジがたってしまうことがある。またオープンエリアも広いため，プラークの内腔突出に注意が必要であるが，内腸骨動脈をまたぐ場合などには血流を阻害することが少ない点で優れると思われる。一方，SMARTではブリッジ本数が多いがベンドの長さが短いため，結果としてLuminexxと同等の柔軟性を有していると考えられる。また，Luminexxよりもオープンエリアは狭いため，プラークの内腔突出に関しては有利であろう。ただし，Luminexxのデリバリーシステムにみられるチップレス構造はステント留置後のデリバリーシステム抜去時の引っかかりがなく，ステントを誤って移動させてしまう

とがない．また，チップの脱落といった事故が起こらないことは大きな利点である。また，最近SelfX（図1E）が保険認可されたが，これはオープンエリアの小ささはSMARTに近く，ブリッジの本数が少ない点はLuminexxに近い。ただし，各々にデザインは異なるため，屈曲時や伸展時などの特性は異なる。

これらのステントの使い分けは様々な議論があると思われるが，閉塞病変ではプラーク量が多くプラークの内腔突出のリスクも増えると考えられるため，我々はオープンエリアが小さいステントを選択するようにしている。また，病変とは反対側からcross overにアプローチをする際は，短縮が少ないステントを選択する事と，デリバリーシステム抜去時のリスクを減らす事を念頭に置きデバイスを選択したり，また前拡張を行ったりしている。

2）大腿動脈

基本的にはTASC A，Bの病変が適応となると考えられる。また，ステントは大腿動脈では適応外使用となるため，バルーンPTAでの早期再狭窄や急性閉塞のリスクがある場合にのみ使用するのが原則である。ナイチノールステントは開存率を改善させるとの報告がある[9]が，それを基材としたdrug eluting stentでの結果が芳しくないものであったこと[6]を考えるとこの領域におけるステントの使用には現在のところ慎重にならざるを得ない。カッティングバルーンは本邦における代替手段であるが，邦人の血管は細い事も多く，ペリフェラル・カッティングバルーンでは径の不適合となることもある。やはり，基本は低圧・長時間の拡張ということになると考える。

3）膝窩動脈

大腿動脈と基本的に同じだが，屈曲部になるためステントの使用はさらにむずかしくなる。大腿動脈の場合は深大腿動脈が側副路として発達している事も多く，重症化することは少ないが，膝窩動脈の閉塞では側副路の発達が不十分で症状が強い場合も多い。また，外科的処置をするにしても関節部で術後瘢痕による機能障害が起こることもあり，治療が難しい場所でもある。虚血症状が強い場合に限り，我々は治療を行っている。

4）下腿動脈

いわゆる跛行趾ではなく，安静時疼痛や潰瘍を有する症例での救趾目的での治療となる。対象となる血管が細く，閉塞病変が多いため，治療が難しい領域でもある。この領域においてsubintimal angioplastyはひとつの選択枝だが，末梢で真腔に抜けているかどうかの判断が難しい場合も少なからずある。この場合には超音波断層撮影装置を併用するのが望ましいと思われる。バルーン径はまず3mmを使うようにしているが，場合によっては5mmぐらいまでバルーン径を大きくすることもある。正確な対象血管径を測定しにくいのも，この領域の特徴だが，経験的には他部位より過拡張に対し強い印象がある。

❸ 閉塞部の通過に関して

最後に閉塞部の通過に関して記すが，スティレートや椎骨動脈型などのように先端に少しアングルがついたカテーテルをバックアップとしてガイドワイヤを先行させて，カテーテルを追従させてゆく。ガイドワイヤの選択には術者によって種々の方法があるが，我々は0.035inch親水性コーティーングのガイドワイヤを用い，先端はストレートとアングル型を使い分ける。腸骨動脈の場合，逆行性に通過が困難な場合は順行性アプローチも試みるが，閉塞部内でキャッチングしワイヤを誘導する事もある。腸骨動脈でもsubintimal recanalizationの報告もある[17]が，大腿動脈以下と異なり出血性合併症が生じた場合に重症となる可能性が高いと思われ，原則的には血管腔内の再開通を行うべきであろう。

文　献

1) Dormandy JA et al：Management of peripheral arterial disease（PAD）. TASC Working Group. TransAtlantic Inter-Society Consensus（TASC）. J Vasc Surg 31（1 Pt 2）：s1-s296，2000

2) Murphy TP et al：Aortoiliac insufficiency；long term experience with stent placement for treatment. Radiology 231：243-249，2004